Development of ferroelectricity in the smectic phases of 4-cyanoresorcinol derived achiral bent-core liquid crystals with long terminal alkyl chains

S. P. Sreenilayam,[1] Yu. P. Panarin,[1,2] J. K. Vij,[1,*] A. Lehmann,[3] M. Poppe,[3] and C. Tschierske[3]

[1]*Department of Electronic and Electrical Engineering, Trinity College Dublin, The University of Dublin, Dublin 2, Ireland*
[2]*School of Electrical and Electronic Engineering, Dublin Institute of Technology, Dublin 8, Ireland*
[3]*Institute of Chemistry, Martin-Luther-University Halle-Wittenberg, Germany*
(Received 15 April 2017; published 16 August 2017)

Bent-core molecules can form numerous polar and symmetry broken liquid crystalline phases with fascinating properties. Here we report the characteristics of a previously unknown polar synclinic smectic phase, $SmC_S P_X$, found in the phase sequence of an achiral bent-core material with a 4-cyanoresorcinol bisbenzoate core, terminated by long linear alkyl chains ($n = 18$) on both ends. This phase exists over a narrow range of temperatures and is sandwiched in between the random polar synclinic smectic phase ($SmC_S P_R$) and polar synclinic ferroelectric ($SmC_S P_F$) phase with $\boldsymbol{P}_S \sim 250 \, \text{nC/cm}^2$. In a planar-aligned cell it exhibits only chirality flipping on application of a conventional ac field but it also exhibits optical switching by rotation of the molecular directors on the tilt cone subjected to a modified sequence of bipolar pulses. This changeover is discussed in terms of the model given by Nakata *et al.* [Phys. Rev. Lett. **96**, 067802 (2006)], involving a competition between the two forms of switching: the rotation around the long molecular axis and the switching through rotation of the molecular directors on the tilt cone. The model is modified to take account of the azimuthal pretilt and the molecular tilt angles. In addition to it, characteristics of $SmC_S P_R$ are also discussed.

I. INTRODUCTION

Liquid crystals (LCs) characterized by fluidity and long-range order [1,2] belong to a fascinating branch of soft condensed matter science. Bent-core LCs have recently been extensively investigated; they exhibit a large variety of phases with a set of unique properties. Some of their characteristics are the following: polar order, spontaneous breaking of the mirror symmetry, and polar switching by electric fields. Bent-core LCs display a multitude of desirable properties while confined in cells with a thickness of the order of a few micrometers. Some of these characteristics form the basis of a range of applications currently being developed [3–12]. In smectic phases of bent-core LCs, the mirror symmetry is broken by the orthogonal combination of tilt and polar direction and there exist different modes of correlations of tilt and polar direction in the neighboring layers. This in turn leads to a rich polymorphism of the polar smectic phases. These include orthogonal smectics where the plane formed by the long molecular axis and the polar director is parallel to the layer normal [13–21]. In most other smectic phases, the plane of the bent-core molecules is tilted to form smectic C (SmC) type phases; the tilt is either left or right from the layer normal and this leads to the formation of several additional subphases [22]. The main difference between the polar smectic phases of bent-core molecules ($B2$ phases) and the nonpolar tilted SmC phase of normal rodlike molecules is that unlike the latter, different molecular configurations can exist among the neighboring layers with synclinic/anticlinic molecular arrangements with respect to the tilt direction and synpolar/antipolar with respect to the polarization vector. Furthermore, these subphases exhibit ferroelectric (F)/antiferroelectric (A) properties. Their structures are described as $SmC_S P_F$, $SmC_A P_A$, $SmC_S P_A$, and

$SmC_A P_F$ [22] (Fig. 1), where C_S stands for a synclinic and C_A for an anticlinic tilt correlation in adjacent layers: P_F and P_A indicate the same and opposite directions of polar order in adjacent layers, respectively.

The bent-core molecules **1/n**, being reported here, consist of five aromatic rings with a central 4-cyanoresorcinol core. This bent 4-cyanoresorcinol core is connected with terephthalate-based arms terminated by identical alkyl chains ($C_n H_{2n+1}, n = 16, 18$) at both ends as shown in Fig. 2 [23]. A common feature of these 4-substituted resorcinols is the "reduced bent angle" compared to the other bent-core mesogens without the 4-substituent [24]. In compounds **1/n**, the peripheral COO groups are reversed with respect to the previously reported series of 4-cyanoresorcinols involving 4-hydroxybenzoate rods, showing exclusively N_{CybC} (cybotactic nematic phases composed of SmC clusters) and SmC phases with larger tilt [25] compared to the compounds of the series **1/n**. This inversion of the peripheral COO groups leads to increased mesophase stability, enhanced polar order, and the reduced tilt for compounds **1/n**. The lower tilt angle gives rise to unusual features and different characteristics that result from a combination of reduced coherence length of the polar order and a weak interlayer coupling. These special features lead to complex phase sequences with transitions between tilted and nontilted phases. A strong influence of confinement and of sample history is found on the phases with different molecular arrangements [23,26–29] and on the dependence of the induced tilt on the electric field [28].

In this paper we focus specifically on the two compounds of the series **1/n** with longest alkyl chains, synthesized so far. Figure 2 lists the phase sequences and transition temperatures of the homologs with $n = 16$ and 18. In previous investigations of **1/16** and **1/18**, we focused on the spontaneous or field-induced development of a helical superstructure in the $SmC_S P_F$ phase and the fast electro-optical switching [30]. Herein we investigate the characteristics of a complete series
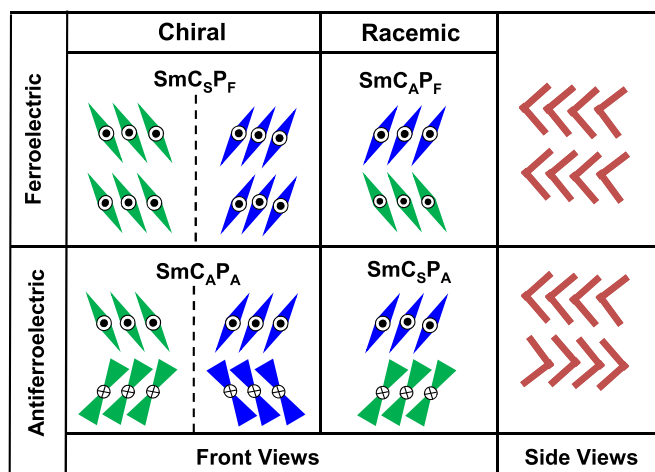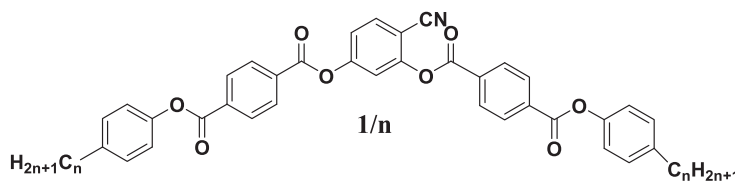
*Corresponding author: jvij@tcd.ie

FIG. 1. Distinct views on the four subtypes of tilted polar smectic phases resulting from the correlation of the tilt and the polar directions (in the front views indicated by dots and crosses) of the bent-core molecules in adjacent layers [22]. The front views represent projections of bent-core molecules with the tip of the molecules in the direction "in" or "out" of the plane. The tip direction is coupled with the polar direction; dots and crosses indicate the polar direction pointing "out" and "into" the plane, respectively. An orthogonal combination of tilt and polar order leads to a reduced C_{2v} symmetry and superstructural chirality of layers (color indicates chirality sense). The notations P_A and P_F refer to the antiferroelectric and ferroelectric polar order; C_A and C_S refer to the anticlinic and synclinic tilt in adjacent layers. The chiral arrangements have two chiral domains separated by a dashed vertical line on the left of this figure.

of distinct paraelectric and polar smectic phases in more detail and thereby find a phase which appears only in a narrow temperature range, sandwiched in between the polarization randomized $SmC_S P_R$ and the polar $SmC_S P_F$ phases of compound **1/18**. The main focus of the present paper will be on this phase, tentatively designated as $SmC_S P_X$. We demonstrate switching of chirality in the $SmC_S P_X$ phase by "chirality flipping" as well as by rotation of the molecular director on the tilt cone depending on the form and the magnitude of the external electric field applied to the cell. In the $SmC_S P_R$ phase, both polarization P and the permittivity $\Delta\varepsilon$ show critical behavior on approaching $SmC_S P_F$, similar to those exhibited by de Vries smectics during the cooling process.

II. EXPERIMENT

Experimental measurements are carried out on homeotropic and planar-aligned LC cells. Homeotropic alignment in a cell is obtained by coating the polymer AL60702 (JSR Korea) on the two indium tin oxide (ITO) coated glass substrates. The substrates are baked at a temperature of 210 °C for 15 min each. A uniform polymer layer of several nanometers thick is adhered on to the substrate. ITO coating on the glass substrate that forms the bottom plate of the cell is etched to form two in-plane electrodes with a spacing of $\sim$80 μm in between the two electrodes. An electric field at a frequency of 110 Hz is applied across these electrodes. Planar alignment in a cell is achieved by coating the substrates with RN1175 polymer (Nissan Chemicals, Japan) and baking these at a temperature of 250 °C for 30 min. The cell thickness controlled by Mylar spacers is measured using an optical interference technique. The cell is mounted in a hot stage, fixed onto the rotating table of the polarizing optical microscope (Olympus BX 52). Temperature of the hot stage is controlled by a Eurotherm 2604 temperature controller to an accuracy better than $\pm$0.05 °C. To investigate the electro-optic behavior of LC phases at higher fields, an electric signal from an Agilent 33120A signal generator amplified by a high voltage amplifier (TReK PZD700) is applied across the electrodes. Measurements of the dielectric permittivity and dielectric loss are made on a planar-aligned cell using a broadband Alpha high resolution dielectric analyzer (Novocontrol GmbH, Germany) in the frequency range of 1 Hz to 10 MHz and by applying a weak electric field. Dielectric cells are made up of two ITO coated glass substrates with a low sheet resistance of the ITO layers (20 $\Omega/\square$). Both ITO covered substrates are spin-coated with a thin planar-alignment layer using the procedure described above in this section. A parastic circuit includes the capacitance of the cell containing the compound in series with a low sheet resistance, R, of the ITO electrodes. The product of R and C must ensure that the frequency of this arrangement $f = 1/(2\pi RC)$ is shifted beyond the desired experimental window of dielectric measurements.

III. RESULTS AND DISCUSSION

A. Polarizing optical microscopy and electro-optical response study of compound 1/18

The texture of the SmA phase of **1/18** in a homeotropic cell (at $T = 135.5$ °C), formed on cooling the sample from the

Compd.	$T/°C$
1/16 (n =16)	Cr 77 Sm$C_A P_A$ 90 Sm$C_S P_F^{hel}$ 110 Sm$C_S P_R$ 125 SmA 162 Iso
1/18 (n =18)	Cr 76 Sm$C_A P_A$ 90 Sm$C_S P_F$ / Sm$C_S P_F^{hel}$ 110.2 Sm$C_S P_X$ 110.7 Sm$C_S P_R$ 134 SmA 160 Iso

FIG. 2. Molecular structure of the investigated bent-core molecules; their mesophases and phase transition temperatures as observed on cooling from the isotropic liquid. Abbreviations: Iso: isotropic state; Cr: crystal; SmA: nontilted and nonpolar smectic phase; Sm$C_S P_R$: paraelectric smectic phase with uniform (synclinic) tilt and almost randomized polar direction of ferroelectric domains; Sm$C_S P_F^{hel}$: synclinic tilted ferroelectric smectic phase with a short pitch where the helical axis lies parallel to the layer normal; Sm$C_A P_A$: anticlinic tilted smectic phase with antiferroelectric polar order.
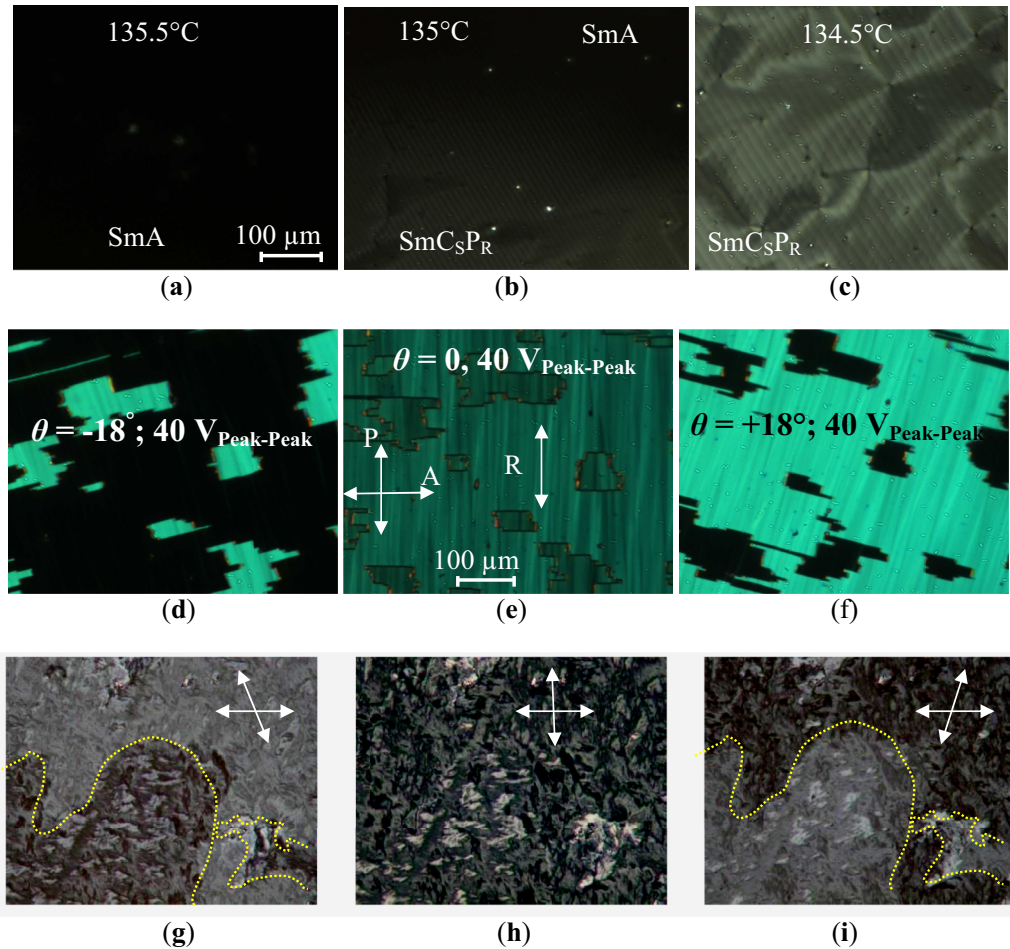
FIG. 3. (a)–(c) Polarizing microphotographs of the SmA and Sm$C_S P_R$ phases recorded under cooling in the absence of an external electric field in a homeotropic ITO cell of cell thickness 6.5 μm filled with **1/18**. (d)–(f) Sm$C_S P_R$ phase at 113 °C in an 8-μm planar-aligned cell; the textures are recorded by application of a 40 $V_{Peak-Peak}$ signal at a frequency of 110 Hz between the ITO coated electrodes; the rubbing direction **R** is (e) along the polarizer or is oriented at an angle θ, (d) $\theta = -18°$, and (f) $\theta = +18°$ to the polarizer. (e) **R** is along the polarizer **P**. (g)–(i) Sm$C_S P_R$ phase at $T = 120$ °C in a homeotropic cell between ordinary glass plates showing chiral domains with opposite handedness, (h) between crossed polarizers, and (g) and (i) with the polarizer rotated by 20° off the 90° position with respect to the analyzer, either in a clockwise or an anticlockwise direction; the brightness of domains is exchanged in (g) and (i), whereas rotation of the cell between the crossed polarizers does not lead to a change in the brightness; these observations indicate a conglomerate of chiral domains with opposite sign of optical rotation in the distinct domains. In the lower part of (b), stripes though similar to (c) are not clearly visible in the figure.

isotropic state, is dark [Fig. 3(a)]; this reflects uniaxiality of the phase. On reducing the temperature to 135 °C [Fig. 3(b)], parts of the cell show Schlieren texture. At 134.5 °C, a fully developed low-birefringent Schlieren texture is observed in a homeotropic cell [Fig. 3(c)], indicating that the transition to an optically biaxial mesophase has occurred. There is a striking pattern of equidistant stripes appearing across the developing Schlieren texture [Figs. 3(b) and 3(c)] which disappears on further cooling. This kind of stripe texture is typically observed for SmA-SmA_b [31] and SmA to SmC_A transitions [32]. This could indicate that the SmA-Sm$C_S P_R$ transition occurs via an additional small range of an intermediate randomized SmC_S domain structure with predominantly anticlinic tilt correlation between the domains [33] before this correlation becomes synclinic in the Sm$C_S P_R$ range. However, since an additional phase transition is not evident from other investigations [polarizing optical microscopy (POM) of planar

samples, differential scanning calorimetry, x-ray diffraction, dielectrics], at the present state of knowledge the stripe pattern is considered as a kind of pre-or post-transitional phenomenon. A typical SmC_S domain texture in a planar cell is recorded at a temperature of 113 °C [Fig. 3(e)]. The texture shows dark and bright areas [Figs. 3(d) and 3(f)] due to two tilt domains where director orientations are inclined at angles $\theta \approx \pm 18°$ to the layer normal. In addition, four-brush disclination points dominate in the Schlieren textures in a homeotropic aligned cell [Fig. 4(a)]. These observations show that the phase under discussion has a uniform molecular tilt in layers, thus belonging to a family of synclinic tilted smectic mesophases (SmC_S). When an electric field is applied across a planar-aligned cell at a temperature of 113 °C [Figs. 3(d)–3(f) in Sm$C_S P_R$ and also in Figs. 6(a) and 6(b)(1)], the texture does not respond to the field, i.e., no optical switching occurs on the application of an electric field. The transition SmA-Sm$C_S P_R$
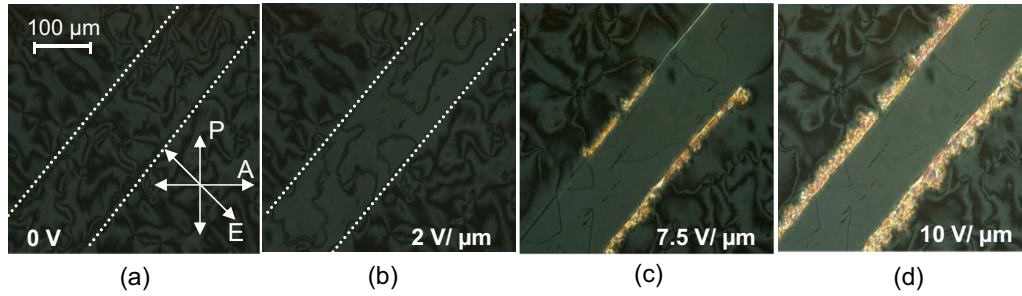
FIG. 4. Polarizing optical microscopic textures of $SmC_S P_R$ phase of compound **1/18** at 113 °C. (a)–(d) show the textures recorded in a 6.5-μm homeotropic aligned cell on the application of an in-plane electric field (E) at a frequency of 110 Hz, applied between the electrodes (the edges of electrodes are indicated by dashed white lines). The in-plane electrodes are fixed at an angle of 45° to the analyzer (A)/polarizer (P) as shown in (a). The distance between the two ITO electrodes is 180 μm.

is continuous and does not involve a measurable value of the transition enthalpy [30]. The $SmC_S P_R$ phase is often referred to as SmC because both phases possess the same C_{2h} symmetry. Nevertheless, the physical characteristics of the $SmC_S P_R$ and SmC phases are very different from each other. In contrast to the nonchiral SmC phase, the $SmC_S P_R$ phase shows properties related to polar phases. For example, a current response to an applied electric field is due to the polar switching [30], and electric-field-induced polarization and soft modelike behavior of the tilt fluctuations are observed on approaching the polar $SmCP$ phases. Some of these observations follow from results of dielectric measurements to be discussed later in the section on dielectric spectroscopy (Sec. III C). Chiral domains are observed under certain conditions in homeotropic aligned cells [see Figs. 3(g)–3(i)] which is typical for $SmC_S P_R$ phases [34] and confirms the tilt of the molecules, because only in this case the layer chirality can develop.

The birefringence of the Schlieren texture continuously increases under cooling and this is clearly reflected in the visual textural changes. When an in-plane electric field at a frequency of 110 Hz is applied at an amplitude of 10 V/μm in a homeotropic cell at a temperature of 113 °C, the initial Schlieren texture [Fig. 4(a)] transforms to a uniform one [Fig. 4(c)] and the birefringence increases with the field [Fig. 4(d)]. On removal of the electric field, the high birefringent state [Fig. 4(d)] returns to a low-birefringent one with Schlieren texture [Fig. 4(a)]. This indicates that a field-induced polar order parallel to the layer planes exists, and the electric field-induced $SmC_S P_F$ state in Fig. 4(d) relaxes to the polarization randomized $SmC_S P_R$ one upon the removal of electric field.

On cooling the homeotropic cell below 113 °C the birefringence starts decreasing. The four-brush Schlieren texture [Fig. 4(a)] at 113 °C slowly changes to a mosaiclike appearance [Figs. 5(a) and 5(b)] at temperatures of 111 °C and 110.8 °C, before reaching the optically uniaxial state [Fig. 5(c)] at 110.5 °C. On further cooling, the high temperature low biaxial phase ($SmC_S P_R$) transforms to a low temperature high
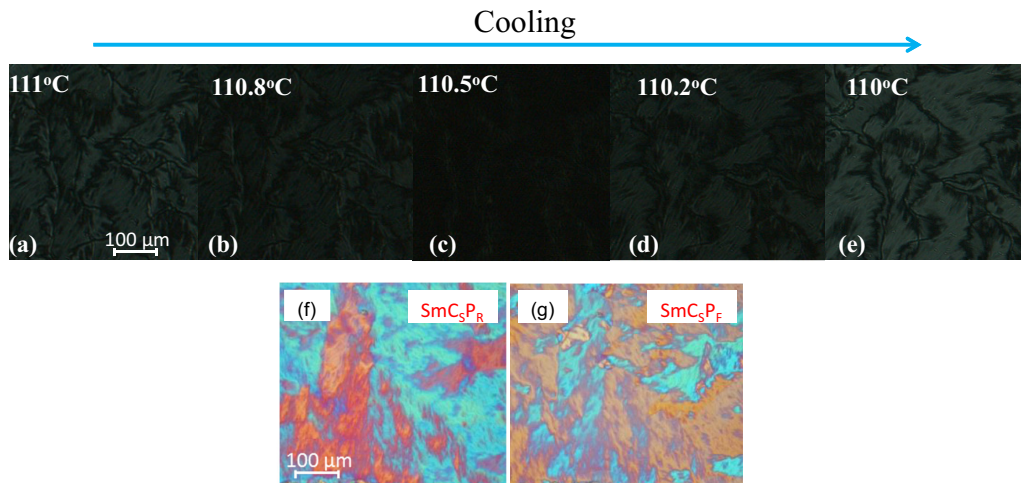

FIG. 5. Polarizing microphotographs of the LC phases of compound **1/18** in a homeotropic aligned cell ($d = 6 \mu$m): (a) $SmC_S P_R$ at 111 °C, (b) 110.8 °C, (c) $SmC_S P_X$ at 110.5 °C, (d) $SmC_S P_F$ at 110.2 °C, and (e) 110 °C. Textures are recorded during the cooling process. To obtain textures (f) and (g) an additional λ-retarder plate is inserted in the homeotropic cell between the crossed polarizers at temperatures of (f) 120 °C and (g) at 100 °C; the last two figures indicate an inversion of birefringence.
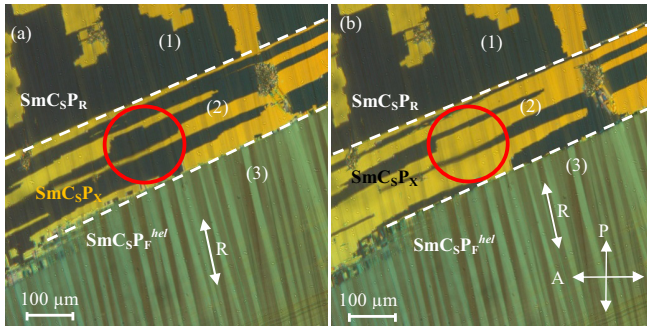
FIG. 6. Polarizing optical microscopic textures of the LC phases of compound **1/18** recorded in a small temperature gradient planar-aligned ITO coated cell of 8 μm cell thickness from higher temperature (top) to lower temperature (bottom): $SmC_S P_R$ (1) $SmC_S P_X$ (2) and $SmC_S P_F^{hel}$ (3). An external field is applied across the two electrodes. The cell is kept at a temperature of $110.5\,^\circ$C and the area (2) in (a) and (b) corresponds to $SmC_S P_X$ phase showing two bistable states, switched oppositely by reversing the polarity of the applied field via an intermediate short-circuited state, respectively. The red circle in (a) and (b) shows an aperture/area of the cell used for the electro-optical measurements. The white dashed lines in (a) and (b) separate out the $SmC_S P_R$, $SmC_S P_X$, and $SmC_S P_F^{hel}$ phases.

biaxial $SmC_S P_F$ phase at $110.2\,^\circ$C [Fig. 5(d)] and $110.0\,^\circ$C [Fig. 5(e)].

A birefringence inversion is demonstrated by inserting an additional λ-retarder plate in between the crossed polarizers [see Figs. 5(f) and 5(g)]. This inversion is due to the flipping of the secondary optical axis [29]. An appearance of the optical uniaxiality is considered as an indication of the formation of an intermediate structure, provisionally labeled here as $SmC_S P_X$. The temperature range of this $SmC_S P_X$ phase is narrow and is restricted to lie only within $\sim$0.5$\,^\circ$C. For this reason, three structures corresponding to $SmC_S P_R$, $SmC_S P_X$, and $SmC_S P_F$ are observed simultaneously in a small temperature gradient cell [Figs. 6(a) and 6(b) at $U = 0$ V]. The sequence of structures is $SmC_S P_R$ (1), $SmC_S P_X$ (2), and $SmC_S P_F$ (3) as temperature decreases from the top to the bottom of the cell. The application of a conventional ac or dc voltage signal does not affect the textures in areas (1) and (2) of the cell, corresponding to $SmC_S P_R$ and $SmC_S P_X$, respectively. On the other hand, in the $SmC_S P_X$ temperature range, an electric current flows on reversing the electric field which demonstrates polar switching brought about by the field. A sudden reversal of the applied field causes reorientation of the polarization or polar vector around the long molecular axis (the so-called "chirality flipping" [35–38]) rather than the director switching on the tilt cone.

It must be stressed that the optical switching in the temperature range of $SmC_S P_X$ can be achieved only by reversing the polarity of the applied field through an intermediate state, short-circuiting the electrodes of the cell [Fig. 6(a)$\rightarrow$6(b); region (2)]. A reversal in the polarity through short-circuiting over a short period of 0.5 ms brings about both electrical and optical switching. The latter can only occur when the director rotates around the tilt cone. On the removal of the electric field, the optical texture returns to its previously switched state, thus showing bistability at $E = 0$ [Fig. 6(b)$\rightarrow$6(a); region (2)]. Such a phenomenon of optical and electric switching under

special conditions has not been reported so far in the literature and reasons for it are being given below.

In order to investigate the electro-optical response of the sample in the $SmC_S P_X$ phase, a successful conduction of the experiment requires additional precautions to be observed since (i) the temperature range of this phase is quite narrow as stated previously, and (ii) the two opposite $\pm\theta$ domains coexist over an area smaller than the minimal aperture of the electro-optical setup. Nevertheless, it is possible to select an area of the cell that corresponds to an almost single domain, as shown by red circles in Figs. 6(a) and 6(b) such that the average transmittance level over the aperture of Fig. 6(a) is less than that of Fig. 6(b). Figure 7 shows a corresponding plot of electrical and optical signals to the oscilloscope screenshots that were recorded for the electro-optical response to the wave form of an applied voltage signal. As already stated, $SmC_S P_X$ phase surprisingly shows a polarization switching current but does not optically react to the square-wave signal applied except for the short spikes that appear on the polarity reversal, shown in Fig. 7(a). On considering the importance of the short-circuited state of optical switching, we modify the applied voltage wave form by a sequence of bipolar square pulses separated by a zero-voltage signal existing over relatively short times (i.e., short-circuit), t_0. Such a modified voltage wave form with a short-circuiting over a time-duration of 0.5 ms causes the full electro-optical switching to occur. This wave form designed for the specific purpose is shown in Fig. 7(b) with 25 ms/div time scale and is expanded to a wave form of 1 ms/div shown in Fig. 7(c).

The switching dynamics was modeled theoretically in bent-core LCs in $B1$ [38] and $B2$ [39] phases. They considered two competing mechanisms of ferroelctric switching: (i) collective rotation around the long molecular axis and (ii) collective rotation around the tilt cone. The electro-optic response in $B2$ phases with temperature and electric field can satisfactorily be explained by the model of Nakata *et al.* [39] which considers two opposite chirality states separated by an energy barrier $U_{\max}\cos^2(\beta)$. This model also considers two competing mechanisms of switching: (a) chirality flipping due to the molecular rotation around its long molecular axis by an angle β and (b) the optical switching due to rotation of the molecular director on the tilt cone by an angle φ. The two dynamical states were modeled by a system of coupled differential equations. These are solved numerically using the Euler-Cauchy method [39]. A key feature of this solution is that both angles start changing from 0 to π on the reversal of the applied electric field. The final switching achieved either by chirality flipping or by the optical switching depends on which one of the two angles, φ or β, reaches the $\pi/2$ state first. When this angle has reached the $\pi/2$ state, this continues to grow further to π, while the second one returns to its initial value/state.

The experimental results show that for low electric fields ($<E_c$) the optical switching by φ angle is observed. On an increase in the electric field greater than E_c, the LC sample shows β switching [35,36,39]. According to the model [39] the threshold field E_C depends linearly on the energy barrier $U_{\max}$. This model, however, does not explain explicitly the observed temperature dependence of the threshold field. This effect can be explained by the energy barrier $U_{\max}$ depending on the molecular tilt angle θ, which in turn depends on temperature.
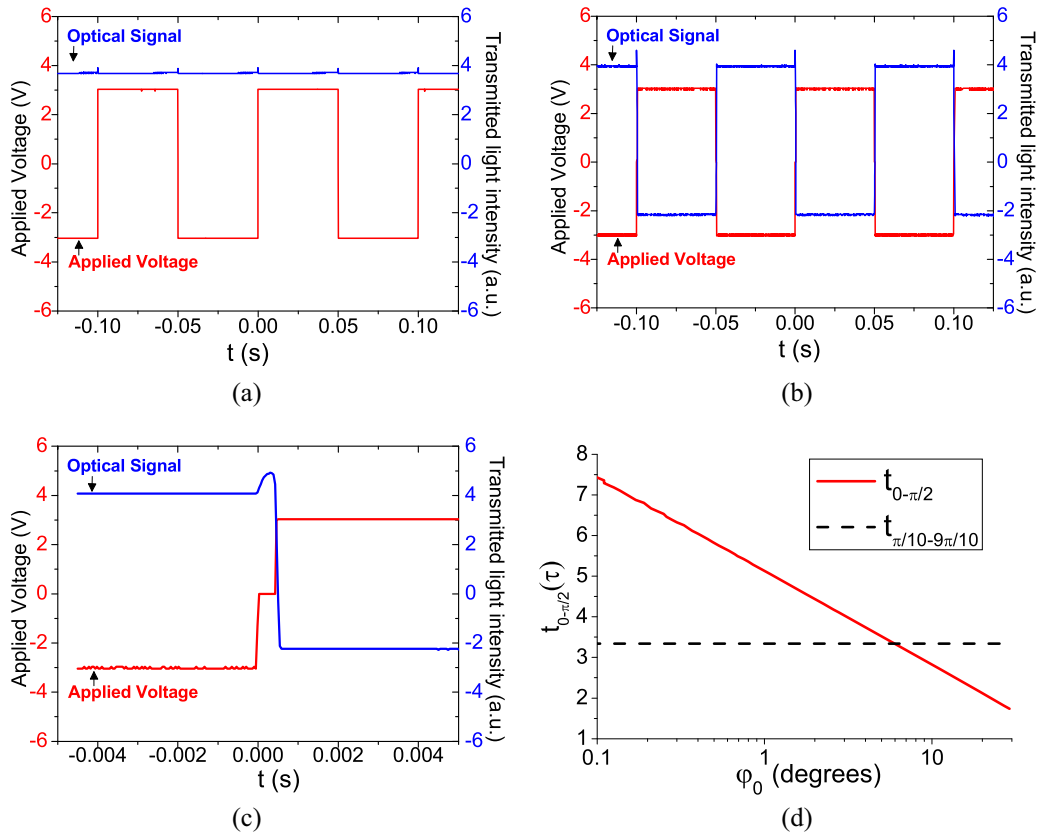
FIG. 7. Electro-optical response of a planar-aligned 8-μm cell, filled with **1/18** in the SmC$_S$P$_X$ phase ($T = 110.5\,°C$), to different applied voltage wave forms (plots of the recorded oscilloscope screenshots): (a) 60 V square wave; (b) 60 V bipolar square pulses, separated by zero voltage over a time duration of 0.5 ms (not seen in the figure for want of high resolution of the abscissa scale) in between the pulses; (c) the same as (b) with time scale expanded to 1 ms/div; (d) the calculated dependence of the switching time on φ from the initial φ_0 state to the critical $\pi/2$ state (solid red line) and from 10% π to 90% π (dashed black line) in the units of τ, where τ is the time constant. The switching time [ordinate in (d)] is found to decrease exponentially with an increase in the initial pretilt angle, φ_0 [abscissa in (d) (φ_0) is plotted on a logarithmic scale]. The ordinate scale for applied voltage in (a) to (c) are to be multiplied by the voltage gain of the amplifier in the experiment which is 20.

Obviously it is zero for $\theta = 0$ and a maximum for $\theta = 90°$, and the energy barrier can be expressed as $U_{\max} = U_0 \sin^2 \theta$. Therefore on an increase in temperature and a consequent decrease in the tilt angle, the energy barrier decreases with temperature. This assists the changeover to chirality flipping (β switching). In the SmC$_S$P$_X$ phase, the energy barrier is low enough to initially provoke "chirality flipping," (due to a small tilt angle $\theta \approx 17°$). However, the optical switching can also be achieved by using a specially designed sequence of pulses [as shown in Figs. 7(b) and 7(c)] and by taking into account the azimuthal pretilt angle.

Earlier Xue *et al.* had discussed the switching of molecular directors on the cone in a ferroelectric SmC* phase consisting of chiral calamitic molecules. They derived analytical solution in *implicit* form, of time t in terms of $\varphi(t)$, the azimuthal angle [40]. Vaksman and Panarin, [41] solved it explicitly in terms of $\varphi(t)$ as a function of t and from it, they found that the delay time t_{0-10} (time taken by the response to go from its initial state of zero to reach 10% of the final response) depends strongly on the initial azimuthal (pretilt) angle φ_0, while the rise time t_{10-90} (the time taken by the response to go from 10% to 90%) is independent of φ_0. In the simplest case of the dielectric anisotropy, measured at low frequencies, and specifically for $\Delta\varepsilon = 0$, the dynamical equation has an exact analytical solution for $\varphi(t)$ [41]. The dependence of the switching of φ from its initial state φ_0 to its critical $\pi/2$ state, $t_{\varphi 0\, to\, \varphi \pi/2} = \log(\pi/2/\tan(\varphi_0/2)) \approx \log(\pi/\varphi_0)$ was found. This is plotted in Fig. 7(d) as a function of φ_0. Based on such a solution, we consider two cases of optical response subjected to (i) a square-wave signal and (ii) a series of bipolar pulses.

In the first case, the switching begins by reversing the polarity of the switched state. The switched state on the application of E makes the pretilt azimuthal angle φ_0 closer to zero due to large polar interactions of P with the field E, ($P \cdot E$). This makes the delay time longer for switching by φ [Fig. 7(d)] and the chirality flipping by β is the only feasible outcome at this stage. In the second scenario, the optical switching by φ begins when the electric field changes from a finite value of E to $E = 0$. In the latter case, the initial pretilt angle φ_0 grows from almost zero value to a finite value depending on the smectic layer tilt δ and the molecular tilt θ as $\varphi_0 = \sin^{-1}[\tan(\delta)/\tan(\theta)]$ [42]. From this equation, the value of φ_0 is found to range in between $10°$ and $20°$ in the bookshelf structure depending on δ and θ but it takes a finite time for the relaxation to occur. The switching delay time [Fig. 7(d)] in this case from φ_0 to $\pi/2$, $t_{\varphi_0 - \varphi \pi/2} \approx 2-3\tau$.
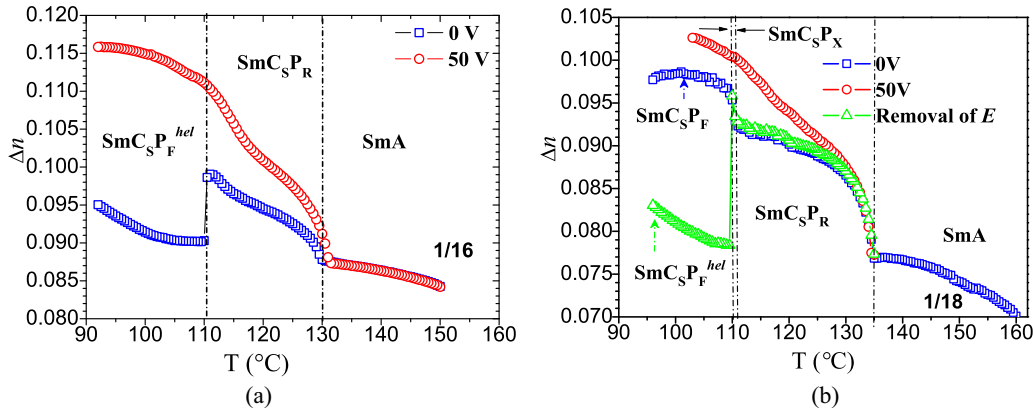
FIG. 8. Temperature and the electric field dependencies of Δn of LC planar-aligned cells filled with (a) **1/16** and (b) **1/18**. The two substrates of a cell are rubbed parallel (**R** on the cell substrates are adjusted as parallel to each other). **R** of a cell is fixed at an angle of $\alpha = 45°$ to the crossed polarizer/analyzer directions. Measurements are carried out on planar-aligned cells under cooling for three different conditions: (i) a virgin state of the cell ($\square$), (ii) under applied electric field ($\circ$) red symbols for both **1/16** and **1/18**, and (iii) on the removal of the applied electric field; ($\triangle$) (green triangle symbol) for **1/18**, whereas for **1/16** the birefringence drops to its zero-field value.

Here φ will reach the critical value of $\pi/2$ prior to β doing the same; the optical switching through φ is then the outcome [Figs. 7(b) and 7(c)]. Hence at the end of the negative pulse, the low initial value of φ_0 relaxes to a higher value at $E = 0$ but it takes a fraction of a millisecond to achieve [see the optical response at $E = 0$; Fig. 7(c)]. When the duration for $E = 0$ is made longer than the relaxation time of φ_0 (~ 0.5 ms, for this case), the optical switching preferably occurs. However, for shorter short-circuited time periods $\ll 0.5$ ms, the chirality flipping takes precedence and in that case chirality flipping is the only feasible outcome.

Summarizing, the POM and the electro-optical studies find that $SmC_S P_X$ is an intermediate uniaxial phase sandwiched in between the $SmC_S P_R$ and $SmC_S P_F$ phases and it has low enough energy barrier for chirality flipping which occurs rather easily. But the optical switching can also be brought about by designing a special sequence of bipolar pulses applied to a planar-aligned cell and this in particular has been demonstrated in this section.

B. Birefringence (Δn) measurements

For carrying out the birefringence (Δn) measurements, the transmitted intensity from a well planar-aligned cell with good alignment is recorded. The rubbing directions **R** on the two substrates are made parallel to each other. **R** is fixed at an angle of $\alpha = 45°$ to the polarizer/analyzer in a crossed polarizers system. The transmitted light (T) through a LC cell as a function of the effective birefringence (Δn_{eff}) is given by [43]

$$T = A \sin^2\left(\frac{\pi \Delta n_{eff} d}{\lambda}\right) + B. \tag{1}$$

Here λ is the wavelength and d is the cell thickness. A is the scaling factor and B is the offset signal. The effective birefringence, Δn_{eff}, exhibits dispersion as a function of λ, the latter is described by modified Cauchy equation [44,45]:

$$\Delta n_{eff}(\lambda) = k_{eff}\left(\frac{\lambda^2 \lambda^{*2}}{\lambda^2 - \lambda^{*2}}\right). \tag{2}$$

k_{eff} and λ^* are the parameters of the Cauchy equation. Equation (2) for Δn_{eff} is inserted into Eq. (1) to take into account the optical dispersion. k_{eff} and λ^* are determined from fits of the transmitted spectrum (T vs λ) at a particular temperature. λ^* so determined is assumed to be a constant over the entire range of temperatures of investigation, whereas k_{eff} is dependent on temperature. The birefringence as a function of temperature is calculated from the transmittance spectra by using this determined value of λ^*. Figure 8 shows Δn, calculated as functions of temperature and voltage from the transmittance data of planar-aligned cells filled with the bent-core LC materials **1/16** (a) and **1/18** (b) both as functions of temperature.

The magnitude of Δn increases on cooling from SmA to the $SmC_S P_F$ phase with characteristic jumps in Δn occurring at each of the phase transition temperatures. Under a square-wave voltage of 50 $V_{Peak-Peak}$ ($f = 110$ Hz), the magnitude of Δn, for both samples **1/16** and **1/18**, increases in the $SmC_S P_R$ and $SmC_S P_F$ phases. In the $SmC_S P_R$ phase, Δn on removal of the electric field is almost equal to the magnitude prior to the field having been applied, for both compounds as is also observed in the textures recorded. In **1/16**, on further cooling from the $SmC_S P_R$ phase, a low-birefringent state is observed and it increases with a decrease in temperature. This phase is assigned as "helical $SmC_S P_F$" ($SmC_S P_F^{helical}$) with a very short helical pitch [30]. It is identical with the previously observed, but not fully investigated, helical $SmC P_\alpha$ phase found for the related compounds with alkoxy chains [29]. It is also related to the weakly tilted or nontilted uniaxial smectic phase with helical rotation of the polar vector, observed for a shorter homolog of the series **1/n** with **n = 14** (also known as PAL 30). In that case, it had been designated as $SmA P_\alpha$, because the tilt was not measurable [17]. The observed low values of birefringence in a planar-aligned cell [Figs. 8(a) and 8(b)] arise from the helical structure that gives rise to a "uniaxial homeotropic texture" [30]. In the $SmC_S P_R$ and $SmC_S P_X$ phases of **1/18** the magnitude of Δn on removal of the electric field is almost equal to its magnitude prior to the application of the field. In the $SmC_S P_F$ phase of **1/18**, the Δn values after removal of the field are much lower than Δn measured prior to the application of the field, in line with the formation of a helix in $SmC_S P_F$ after the cell has been treated by the electric field.

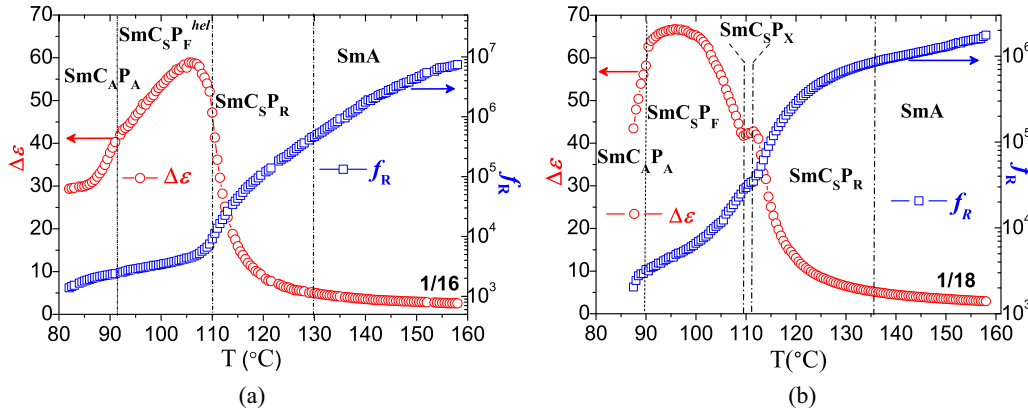FIG. 9. Dielectric relaxation strength $\Delta\varepsilon(\circ)$ and corresponding relaxation frequency f_R ($\square$) for the two samples (a) **1/16** ($d = 8\,\mu$m) and (b) **1/18** ($d = 6.6\,\mu$m) in planar-aligned cells as a function of temperature. Measurements in both cases are carried out under the cooling process.

This can be due to the field-induced weakening/breaking of the synclinic smectic interlayer molecular interactions, which turn out to be stronger in the SmC$_S$P$_F$ phase of **1/18** (tilt, 23°) than in the same phase of **1/16** (with a smaller tilt, 17°). For the latter, the helix is spontaneously formed at the transition to the polar ferroelectric phase, whereas for **1/18** the polar smectic phase requires electric field treatment and in consequence the helical structure is induced in the latter. The helical state once formed/induced is retained even after the field has been removed. This implies that the SmC$_S$P$_F$ phase of **1/18** on transition from SmC$_S$P$_X$ temporarily retains a quasistable (surface stabilized) nonhelical, uniformly polar structure which then transforms to the thermodynamically stable helical state with a short helical pitch. Once formed, the helical state of SmC$_S$P$_F$ does not return or relax back to its initial uniformly polar SmC$_S$P$_F$ state.

The helical state arises as a consequence of the minimization of the electrostatic energy from a large in-layers spontaneous polarization $\boldsymbol{P}_S$ in the SmC$_S$P$_F$ phase. According to a simple phenomenological theory given by Pikin and Indenbom [46], the helical structure in tilted smectics is formed by a large spontaneous polarization and is independent of chirality. The latter determines the sense of the helical winding. For nonchiral LCs, formation of a helical structure reduces the electrostatic energy but at the same time it increases the elastic energy. Stabilization of a helical structure is thus a compromise between these two competing energies: electrostatic and elastic. The helical pitch is expressed as [46]

$$p_0 = \frac{2\pi K\theta}{\mu P_S}, \tag{3}$$

where K is elastic constant, μ is the flexoelectric coefficient, θ is the tilt angle, and P_S is the spontaneous polarization. The relatively small molecular bend angle in the polar smectic phases of compound **1/18** provides a weak polar coupling between the layers, e.g., a lower elastic constant K. Therefore, in weakly tilted and weakly coupled polar smectics with large spontaneous polarization ($\sim$400 nC/cm^2) the ratio K/P_S is very low when compared to the conventional SmC* phase of chiral calamitic molecules. This explains the existence of an

anomalously short helical pitch ($\sim$15 nm) in **1/18** determined using atomic force microscopy (AFM) [30].

C. Dielectric spectroscopy

The complex permittivity $\varepsilon^* = \varepsilon' - i\varepsilon''$ (i is the imaginary number) is measured as a function of frequency and temperature by applying a weak probe electric field to a planar-aligned cell. The experimental values of the dielectric strength ($\Delta\varepsilon$) and the relaxation frequency (f_R) are obtained for samples **1/16** and **1/18** in planar-aligned cells by fitting the experimental dielectric spectra to the Havriliak-Negami equation [47],

$$\varepsilon^*(\omega) = \varepsilon' - i\varepsilon'' = \varepsilon_\infty + \sum_{j=1}^{n} \frac{\Delta\varepsilon_i}{[1 + (i\omega\tau_j)^{\alpha_j}]^{\beta_j}} - \frac{i\sigma_{dc}}{\varepsilon_0\omega},$$

$$\tag{4}$$

where ε_∞ is the high-frequency dielectric permittivity, j varies from 1 to n (where n is the number of relaxation processes), $\omega = 2\pi f$ is the angular frequency, ε_0 is the permittivity of free space, τ_j is the relaxation time, $\Delta\varepsilon_j$ is the corresponding dielectric relaxation strength, and α_j and β_j are the respective symmetric and asymmetric broadening parameters corresponding to the jth process. $\sigma_{dc}/\varepsilon_0\omega$ is the contribution of dc conductivity to ε''. The relaxation frequency, f_j, of the jth process is related to τ_j [48] as

$$f_j = \frac{1}{2\pi\tau_j}\left[\frac{\sin(\alpha_j\pi)}{2+2\beta_j}\right]^{1/\alpha_j}\left[\frac{\sin(\alpha_j\beta_j\pi)}{2+2\beta_j}\right]^{-1/\alpha_j}. \tag{5}$$

The temperature dependencies of $\Delta\varepsilon$ and f_R for the main relaxation process are fitted to Eq. (4), results from which are shown in Figs. 9(a) (**1/16**) and 9(b) (**1/18**), respectively.

The dielectric strength $\Delta\varepsilon$ of the SmC$_S$P$_R$ phase for both **1/16** and **1/18** samples increases gradually with decreasing temperature. This implies a soft modelike increase in the correlations of the neighboring molecules on transition to the polar SmCP phase. The corresponding f_R of the relaxation process decreases with decreasing temperature. In the SmC$_S$P$_R$ phase close to the transition temperature of the SmC$_S$P$_F^{hel}$ (in **1/16**)/SmC$_S$P$_F$ (in **1/18**) phase, the soft
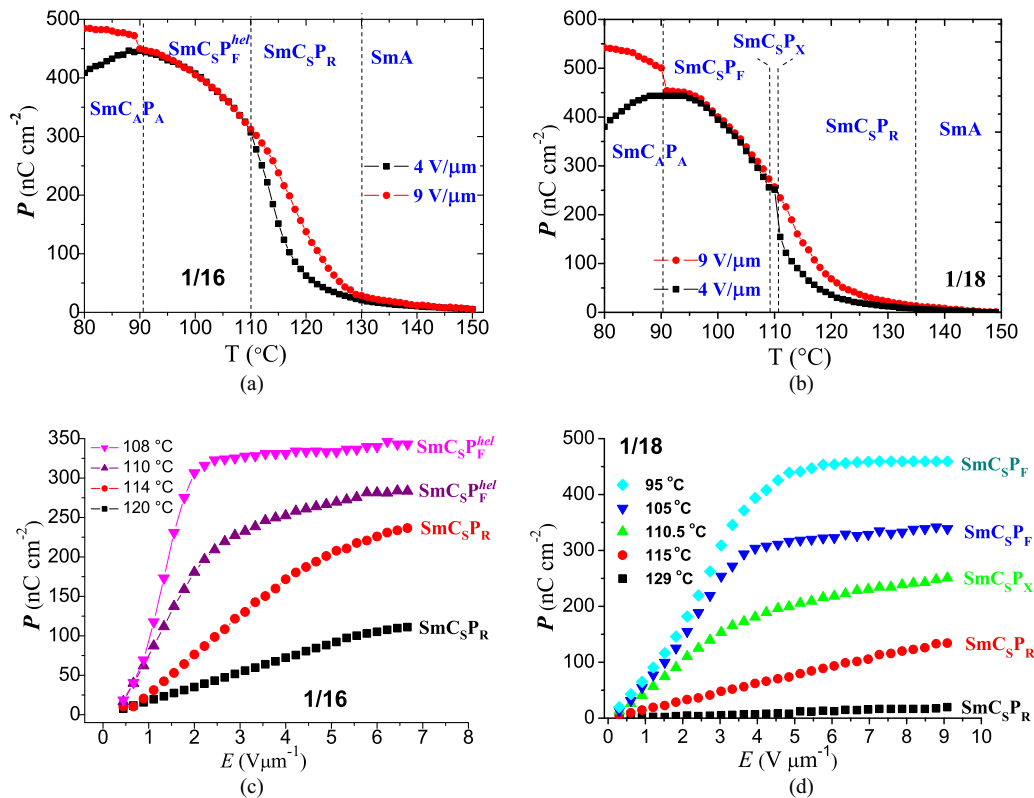
FIG. 10. Temperature and field dependencies of **P** measured in planar-aligned cells (a) and (c) filled with compound **1/16** (9 μm) and (b) and (d) filled with compound **1/18** (6.3 μm). Measurements are carried out by applying a square-wave ac voltage wave form at a frequency of 110 Hz.

mode $\Delta\varepsilon$ sharply increases and f_R sharply decreases. The temperature dependencies of $\Delta\varepsilon$ at the SmC_SP_R to SmC_SP_F are fitted to a power-law equation $\Delta\varepsilon = k/(T - T_c)^\gamma$; exponent γ is found as 1.5 for **1/16**, and 1.55 for **1/18**, both larger than the typical value of $\sim$1.3 found for a conventional SmA-SmC phase transition. Magnitude of the exponent as $\sim$1.5 is reminiscent of the de Vries scenario at the SmA^* to SmC^* transition [49–51]. On further cooling of **1/18** in a planar-aligned cell, we observe a small steplike behavior in a narrow range of temperatures 110.7 °C−110.2 °C (SmC_SP_X) with a magnitude of $\Delta\varepsilon \sim 42.3$ [Fig. 9(b)]. However, in the **1/16** sample [Fig. 9(a)], $\Delta\varepsilon$ increases with a characteristic jump at the SmC_SP_R to $SmC_SP_F^{hel}$ phase transition at 110 °C and then decreases slowly on the formation of a helix. In the $SmC_SP_F^{hel}$ phase of the **1/16** sample, the helix can easily be distorted by a weak external electric field and a change in the macroscopic polarization with the applied field is very significant and the relative permittivity is also large. The rise of $\Delta\varepsilon$ in the SmC_SP_X and SmC_SP_F phases of **1/18** can be explained by a competition between the increase in the polarization and a corresponding escape from the polar order through formation of a helical structure as well as forming antipolar correlations on approaching the SmC_AP_A phase. The latter is also composed of polar layers with polar directions alternating from layer to layer thus resulting in a decrease in $\Delta\varepsilon$. The dielectric behavior both in the dielectric strength and the relaxation frequency is characteristically different from the conventional SmA^* and SmC^* phases of calamitic chiral LCs [52,53].

D. Polarization measurements

Figure 10 shows the temperature and field dependencies of the induced polarization **P** measured using planar-aligned cells, filled with compounds **1/16** and **1/18**. Measurements are carried out in the cooling process under application of a square voltage wave form of frequency 110 Hz using the method reported previously [41,42].

The shape of the polarization curves [Figs. 10(a) and 10(b)] as a function of temperature at electric fields up to 9 V/μm is similar to the observed temperature dependencies of dielectric strength $\Delta\varepsilon$ [Figs. 9(a) and 9(b)]. In SmC_SP_R, both **P** and $\Delta\varepsilon$ show critical behavior similar to the de Vries SmA^* to SmC^* transition but different from the conventional SmA^* to SmC^* transition. In this phase, the measured polarization is electric-field induced and hence is field dependent. However, in the SmC_SP_X ($\sim$250 nC cm^{-2}) and SmC_SP_F phases of **1/18** and in the $SmC_SP_F^{hel}$ phase of **1/16** the **P** value is independent of the field greater than 4 V/μm, hence it is the spontaneous polarization. In the SmC_AP_A phase **P** decreases for low electric fields ($\sim$390 nC cm^{-2} at 80 °C) due to the formation of antiferroelectric order, while at higher electric fields, the ferroelectric state is induced and **P** grows to $\sim$450 nC cm^{-2}.

The field dependencies of **P** are shown in Figs. 10(c) and 10(d). There is a linear increase with the field in the temperature range of SmC_SP_R phase with its slope increasing with decreasing field, in line with that observed for paraelectric switching. In the SmC_SP_F phase, however, there is saturation at a field of 4 V μm^{-1} followed by a plateau. These are the

typical features of polar switching. In the intermediate state, i.e., in the $SmC_S P_X$ range of **1/18**, the field dependency of P is intermediate in between $SmC_S P_R$ and $SmC_S P_F$. In the temperature range of this phase an initial increasing trend in slope of P with temperature registers a decrease at $\sim$4 V μm^{-1} but up to $\sim$9 V μm^{-1} the P (E) curve does not appear to reach a plateau in P.

IV. CONCLUSIONS

A detailed investigation of 4-cyanoresorcinol bisbenzoate bent-core LCs terminated by long alkyl chains, $n = $ **16,18** has been carried out by using a range of experimental methods such as optical polarizing microscopy, electro-optics, birefringence, dielectric, and polarization measurements. Here we present the results of an intermediate $SmC_S P_X$ phase in **1/18** material at the transition from the short- to the long-range polar order in the layers. This phase is an intermediate state and is sandwiched in between $SmC_S P_R$ and $SmC_S P_F$ and is uniaxial. This is found to have low energy barrier for chirality flipping. Due to such a low barrier, the application of an electric field enables chirality flipping to occur, rather than electro-optical

switching on the tilt cone, as observed for the majority of other polar smectic phases. Nevertheless, the $SmC_S P_X$ phase also shows optical switching on application of bipolar pulses separated by short-circuited pulses. This transition from chirality flipping to optical switching is explained by the dynamic model given by Nakata *et al.* [39] where additionally the initial pretilt angle, φ_0, is taken into account. The energy barrier depending on the molecular tilt angle is also taken into consideration. Switching by rotation of the director on a tilt cone is a signature of the transition from the Langevin-type switching in $SmC_S P_R$ to the polar optical switching in $SmC_S P_F$.

[1] P. G. de Gennes and J. Prost, *The Physics of Liquid Crystals* (Clarendon, Oxford, 1993).

[2] S. Chandrasekhar, *Liquid Crystals* (Cambridge University Press, Cambridge, UK, 1992).

[3] R. A. Reddy and C. Tschierske, J. Mater. Chem. **16**, 907 (2006).

[4] H. Takezoe and Y. Takanishi, Jpn. J. Appl. Phys. **45**, 597 (2006).

[5] T. Sekine, T. Niori, J. Watanabe, T. Furukawa, S. W. Choi, and H. Takezoe, J. Mater. Chem. **7**, 1307 (1997).

[6] T. Niori, T. Sekine, J. Watanabe, T. Furukawa, and H. Takezoe, J. Mater. Chem. **6**, 1231 (1996).

[7] S. P. Sreenilayam, Yu. P. Panarin, J. K. Vij, M. Osipov, A. Lehmann, and C. Tschierske, Phys. Rev. E **88**, 012504 (2013).

[8] S. P. Sreenilayam, Yu. P. Panarin, J. K. Vij, S. I. Torgova, A. Lehmann, and C. Tschierske, Phys. Rev. E **92**, 022502 (2015).

[9] E. Westphal, H. Gallardo, G. F. Caramori, N. Sebastian, M.-G. Tamba, A. Eremin, S. Kawauchi, M. Prehm, and C. Tschierske, Chem. Eur. J. **22**, 8181 (2016).

[10] J. Etxebarria and M. B. Ros, J. Mater. Chem. **18**, 2919 (2008).

[11] R. A. Callahan, D. C. Coffey, D. Chen, N. A. Clark, G. Rumbles, and D. M. Walba, ACS Appl. Mater. Interfaces **6**, 4823 (2014).

[12] W. Iglesias and A. Jákli, in *Handbook of Liquid Crystals*, edited by J. W. Goodby, P. J. Collings, T. Kato, C. Tschierske, H. F. Gleeson, and P. Raynes, 2nd ed. (Wiley-VCH, Weinheim, 2014), Vol. 8, pp. 799–817.

[13] A. Eremin, S. Diele, G. Pelzl, H. Nádasi, W. Weissflog, J. Salfetnikova, and H. Kresse, Phys. Rev. E **64**, 051707 (2001).

[14] B. K. Sadashiva, R. A. Reddy, R. Pratibha, and N. V. Madhusudana, J. Mater. Chem. **12**, 943 (2002).

[15] D. Pociecha, M. Čepič, E. Gorecka, and J. Mieczkowski, Phys. Rev. Lett. **91**, 185501 (2003).

[16] K. Gomola, L. Guo, D. Pociecha, F. Araoka, K. Ishikawa, and H. Takezoe, J. Mater. Chem. **20**, 7944 (2010).

[17] Yu. P. Panarin, M. Nagaraj, S. Sreenilayam, J. K. Vij, A. Lehmann, and C. Tschierske, Phys. Rev. Lett. **107**, 247801 (2011).

[18] R. A. Reddy, C. Zhu, R. Shao, E. Körblova, T. Gong, Y. Shen, E. Garcia, M. A. Glaser, J. E. Maclennan, D. M. Walba, and N. A. Clark, Science **332**, 72 (2011).

[19] T. Akutagawa, Y. Matsunaga, and K. Yasuhara, Liq. Cryst. **17**, 659 (1994).

[20] S. Sreenilayam, M. Nagaraj, Yu. P. Panarin, J. K. Vij, A. Lehmann, and C. Tschierske, Mol. Cryst. Liq. Cryst. **553**, 133 (2012).

[21] M. J. O'Callaghan, M. D. Wand, C. M. Walker, and M. Nakata, Appl. Phys. Lett. **85**, 6344 (2004).

[22] D. R. Link, G. Natale, R. Shao, J. E. Maclennan, N. A. Clark, E. Körblova, and D. M. Walba, Science **278**, 1924 (1997).

[23] C. Keith, M. Prehm, Yu. P. Panarin, J. K. Vij, and C. Tschierske, Chem. Commun. **46**, 3702 (2010); N. Sebastian, S. Belau, A. Eremin, M. Alaasar, M. Prehm, and C. Tschierske, Phys. Chem. Chem. Phys. **19**, 5895 (2017).

[24] I. Wirth, S. Diele, A. Eremin, G. Pelzl, S. Grande, L. Kovalenko, N. Pancenkoa, and W. Weissflog, J. Mater. Chem. **11**, 1642 (2001).

[25] C. Keith, A. Lehmann, U. Baumeister, M. Prehm, and C. Tschierske, Soft Matter **6**, 1704 (2010).

[26] A. A. S. Green, R. F. Shao, J. E. MacLennan, M. A. Glaser, N. A. Clark, and C. Tschierske, Investigating the rich phase sequence of PAL30, poster ILCC2016-460, Kent State University, Ohio, July 31 to August 5 (2016) (unpublished).

[27] E. I. Kats and V. V. Lebedev, C1-11 ILCC2016-3 Non-linear fluctuation effects in dynamics of freely suspended films, ILCC2016, electronic abstracts, Kent State University, Ohio, July 31 to August 5 (2016) (unpublished).

[28] H. Ocak, M. Poppe, B. Bilgin-Eran, G. Karanlik, M. Prehm, and C. Tschierske, Soft Matter **12**, 7405 (2016).

[29] M. Alaasar, M. Prehm, M. Poppe, M. Nagaraj, J. K. Vij, and C. Tschierske, Soft Matter **10**, 5003 (2014).

[30] S. P. Sreenilayam, Yu. P. Panarin, J. K. Vij, V. P. Panov, A. Lehmann, M. Poppe, M. Prehm, and C. Tschierske, Nat. Commun. **7**, 11369 (2016).

[31] T. Hegmann, J. Kain, S. Diele, G. Pelzl and C. Tschierske, Angew. Chem., Int. Ed. **40**, 887 (2001); R. Prathibha, N. V. Madhusudana, and B. K. Sadashiva, Europhys. Lett. **80**, 46001 (2007); C. V. Yelamaggad, I. S. Shashikala, V. P. Tamilenthi, D. S. S. Rao, G. G. Nair, and S. K. Prasad, J. Mater. Chem. **18**, 2096 (2008).

[32] S. Radhika, B. K. Sadashiva, and R. Prathibha, Liq. Cryst. **37**, 417 (2010); A. Yoshizawa, M. Kurauchi, Y. Kohama, H. Dewa, K. Yamamoto, I. Nishiyama, T. Yamamoto, J. Yamamoto, and H. Yokoyama, *ibid.* **33**, 611 (2006).

[33] D. Guzeller, H. Ocak, B. Bilgin-Eran, M. Prehm, and C. Tschierske, J. Mater. Chem. C **3**, 4269 (2015).

[34] M. Alaasar, M. Prehm, M. Nagaraj, J. K. Vij, and C. Tschierske, Adv. Mater. **25**, 2186 (2013); M. Alaasar, M. Prehm, K. May, A. Eremin, and C. Tschierske, Adv. Funct. Mater. **24**, 1703 (2014); M. Alaasar, M. Prehm, S. Poppe, and C. Tschierske, Chem. Eur. J. **23**, 5541 (2017).

[35] A. Eremin, S. Diele, G. Pelzl, and W. Weissflog, Phys. Rev. E **67**, 020702 (2003).

[36] M. W. Schröder, S. Diele, G. Pelzl, and W. Weissflog, ChemPhysChem **5**, 99 (2004).

[37] G. Pelzl, M. W. Schröder, A. Eremin, S. Diele, B. Das, S. Grande, H. Kresse, and W. Weisslog, Eur. Phys. J. E **21**, 293 (2006).

[38] E. Gorecka, N. Vaupotič, D. Pociecha, M. Čepič, and J. Mieczkowski, ChemPhysChem **6**, 1087 (2005).

[39] M. Nakata, R.-F. Shao, J. E. Maclennan, W. Weissflog, and N. A. Clark, Phys. Rev. Lett. **96**, 067802 (2006).

[40] J. I. Xue, M. A. Handschy, and N. A. Clark, Ferroelectrics **73**, 305 (1987).

[41] V. M. Vaksman and Yu. P. Panarin, Mol. Mater. **1**, 147 (1992); also see in V. Panov, J. K. Vij, and N. M. Shtykov, Liq. Cryst. **28**, 615 (2001).

[42] Yu. P. Panarin, Y. P. Kalmykov, S. T. Mac Lughadha, H. Xu, and J. K. Vij, Phys. Rev. E **50**, 4763 (1994); Yu. P. Panarin, H. Xu, S. T. Mac Lughadha, and J. K. Vij, Jpn. J. Appl. Phys. **33**, 2648 (1994).

[43] O. E. Panarina, Yu. P. Panarin, F. Antonelli, J. K. Vij, M. Reihmann, and G. Galli, J. Mater. Chem. **16**, 842 (2006).

[44] J. Li and S.-T. Wu, J. Appl. Phys. **95**, 896 (2004).

[45] S. P. Sreenilayam, V. P. Panov, J. K. Vij, and G. Shanker, Liq. Cryst. **44**, 244 (2017).

[46] S. A. Pikin and V. L. Indenbom, Ferroelectrics **20**, 151 (1978).

[47] S. Havriliak, Jr. and S. Negami, Polymer **8**, 161 (1967).

[48] O. E. Kalinovskaya and J. K. Vij, J. Chem. Phys. **112**, 3262 (2000).

[49] A. de Vries, J. Chem. Phys. **71**, 25 (1979).

[50] U. Manna, J.-K. Song, G. Power, and J. K. Vij, Phys. Rev. E **78**, 021711 (2008).

[51] S. P. Sreenilayam, D. M. Agra-Kooijman, V. P. Panov, V. Swaminathan, J. K. Vij, Yu. P. Panarin, A. Kocot, A. Panov, D. Rodriguez-Lojo, P. J. Stevenson, M. R. Fisch, and S. Kumar, Phys. Rev. E **95**, 032701 (2017); N. Yadav, V. P. Panov, V. Swaminathan, S. P. Sreenilayam, J. K. Vij, T. S. Perova, R. Dhar, A. Panov, D. Rodriguez-Lojo, and P. J. Stevenson, *ibid.* **95**, 062704 (2017).

[52] H. Xu, J. K. Vij, A. Rappaport, and N. A. Clark, Phys. Rev. Lett. **79**, 249 (1997).

[53] A. Kocot, R. Wrzalik, J. K. Vij, M. Brehmer, and R. Zentel, Phys. Rev. B **50**, 16346 (1994).